Cryo electron tomography studies of bacterial chemosensory arrays

Yang W.

CHAPTER 4

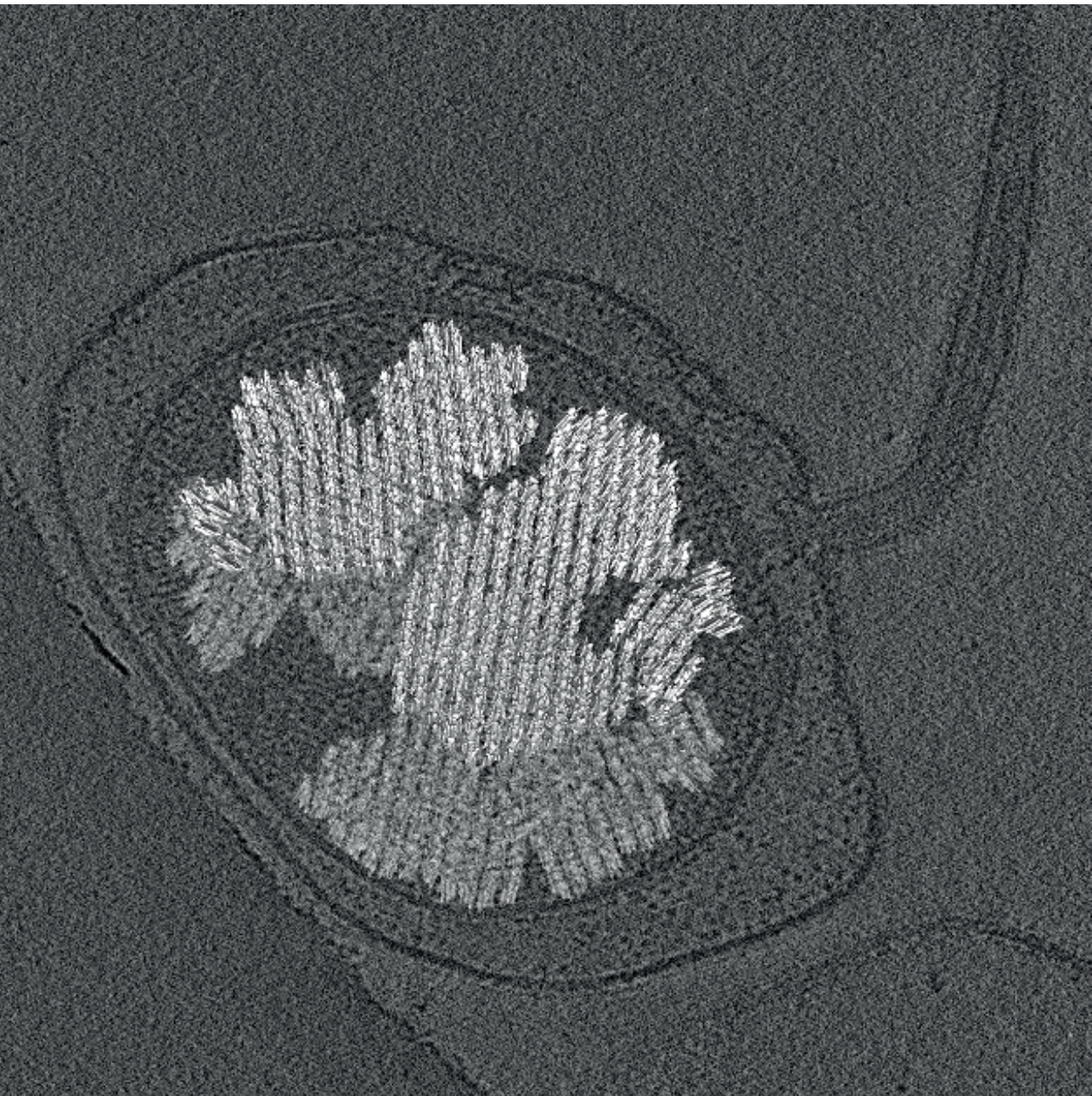

Kinase distribution in *Vibrio cholerae* F6 chemotaxis arrays

Abstract

Chemotaxis is a widespread behavior among motile bacteria that allows the cells to sense chemical changes in the environment and modulate their motility accordingly. The signals are sensed by chemoreceptors that arrange in extended ordered arrays and cluster together with other essential chemotaxis proteins, including CheA, the key enzyme in the signaling pathway. The receptor packing in ordered hexagonal arrays is considered universal among all bacteria and archaea. Despite the conserved receptor lattice, here we show that the molecular architecture of the chemotaxis proteins in the baseplate differ in the F6 arrays in *Vibrio cholerae* compared to its F7 counterpart in *Escherichia coli*. Cryo-electron tomography allows the visualization of the CheA positions in intact arrays of *V. cholerae*. The data reveals that CheA proteins are evenly distributed across the baseplate but lack an ordered arrangement. We propose such a variable distribution of CheA reduces the rigidity of the arrays and thus allows for a more dynamic exchange of different chemoreceptors and the baseplate components, which is the structural basis for a proper chemotaxis function with high cooperativity.

Introduction

Chemotaxis is a behavior most motile bacteria employ that allows the cells to sense their environment and direct their movement towards favorable environmental niches for survival. For the human intestinal pathogen *Vibrio cholerae*, the chemotaxis machinery aids the cells' survival during its life cycle, both in its environmental phase and during host infection (160-165). However, it is difficult to pinpoint the exact role of chemotaxis in *V. cholerae* pathogenicity due to contradictory results (166-170). Nevertheless, changes in chemotactic capability and motility may be associated with vastly altered localization in the host intestine (168, 171, 172).

Given the diverse environments where *V. cholerae* thrives, it is not surprising that their chemosensory system is much more complex than the best-understood model system in *E. coli* (63, 64). *V. cholerae* is equipped with 43 chemoreceptor-encoding genes in its genome. Moreover, *V. cholerae* possess 3 chemotaxis gene clusters, each of which comprises an individual chemotaxis pathway and a structurally distinctive chemosensory array (104, 122, 170, 173). The exact functions of Cluster I and Cluster III chemotaxis pathways remain largely elusive (80, 83). CheA-2, the functional homologue of the histidine kinase CheA in *E. coli*, and CheY-3, which is the only CheY that can directly control the rotation of the single polar flagellum, are both encoded by genes in Cluster II(82, 174). Furthermore, Cluster II chemosensory (also referred as F6 arrays classified based on the evolutionary history), is the only system in *V. cholerae* that appears to control motility (70).

In *E. coli*, membrane-bound chemoreceptors form trimers-of-dimers, which are arranged in a hexagonal lattice, networked at their cytoplasmic tips through rings formed by the P5 domain of the kinase CheA and the coupling protein CheW (43, 44, 47). In *V. cholerae*, the membrane-bound F6 arrays are always located at the flagellar pole (113). These arrays were shown to have a high compositional complexity, which is not only due to the number of different chemoreceptors. The Cluster II arrays also contain additional chemotaxis proteins, such as ParP and CheVs, that can integrate directly into the baseplate in addition to CheW and CheA (112, 151). F6 arrays can still self-assemble and retain native packing order of receptors even in the absence of all three CheAs (102). However, recent work implies that in order to compensate for low abundance or even the total lack of CheA, less frequently used coupling proteins are recruited into the baseplate instead. The stoichiometry of chemotaxis proteins based on proteomics data suggests that CheA abundance is naturally much lower in native *V. cholerae* F6 arrays compared to arrays in *E. coli* (102).

Although we speculated about the structural arrangement of CheA in the baseplate in our previous study, we were not able to visualize its distribution. This was largely due to the thickness of intact *V. cholerae* cells, which is prohibitive for high-resolution imaging. In *E. coli*, this thickness limitation was overcome in previous studies by cell lysis to flatten the cells. The arrays in *E. coli* are known to be ultrastable and the arrays withstand lysis without changes to their ultrastructure. In contrast, the F6 arrays *V. cholerae* tend to lose their native packing order upon cell lysis. However, the arrangement of CheA in the F6 arrays, either in an ordered or disordered fashion, may shed important insights into the formation and function of this system.

In this study we use cryo-electron tomography (cryo-ET) to image the F6 arrays in their native state in *V. cholerae* minicells. We applied subtomogram averaging analysis to determine the kinase distribution in the baseplate of intact F6 arrays. Our structural analysis of baseplate components agrees with the determined abundance of CheA based on the proteomics results reported previously. It further supports that the F6 arrays tolerate a high level of variability of chemoreceptors and chemotaxis proteins.

Results

V. cholerae minicells are suitable system for imaging F6 arrays

V. cholerae are comma-shaped gram-negative bacteria with a diameter between 0.5 – 1.0 microns. These dimensions exceed the practical limit of Cryo-ET to reveal fine structural detail. In this study, we use a derivative strain of *V. cholerae* N16961 with *minCD* and *matP* deletions (175). Strains with one or multiple deletions in the *min* gene cluster are capable of releasing minicells from the cell pole of rod-shape bacteria (176). These achromosomal cells often retain some polar collated machinery, which make them an ideal system for studying chemosensory arrays (43, 44, 177). The minicells have a reduced size with an average diameter of 400 nm (52 minicells imaged in total) (Fig. 1A). The smallest minicells imaged are less than 200 nm in diameter. Chemotaxis arrays can be seen in the tomograms either as a hexagonal lattice (top views) or as a density layer parallel to the inner membrane (side views) (Fig. 1 B&C). Chemotaxis arrays were observed in 65% of all flagellated minicells imaged.

Chemoreceptor lattice in F6 arrays are hexagonally packed

Subtomogram averaging of the chemoreceptor arrays revealed that the receptors form a lattice that spans 23 nm between the baseplate and the inner membrane (Fig. 2A). The distance from the cytoplasmic tips of the receptors that are associated to the baseplate components to the periplasmic domains of the receptors is about 33 nm. The receptors are arranged in the typical hexagonal lattice with a spacing of about 12 nm.

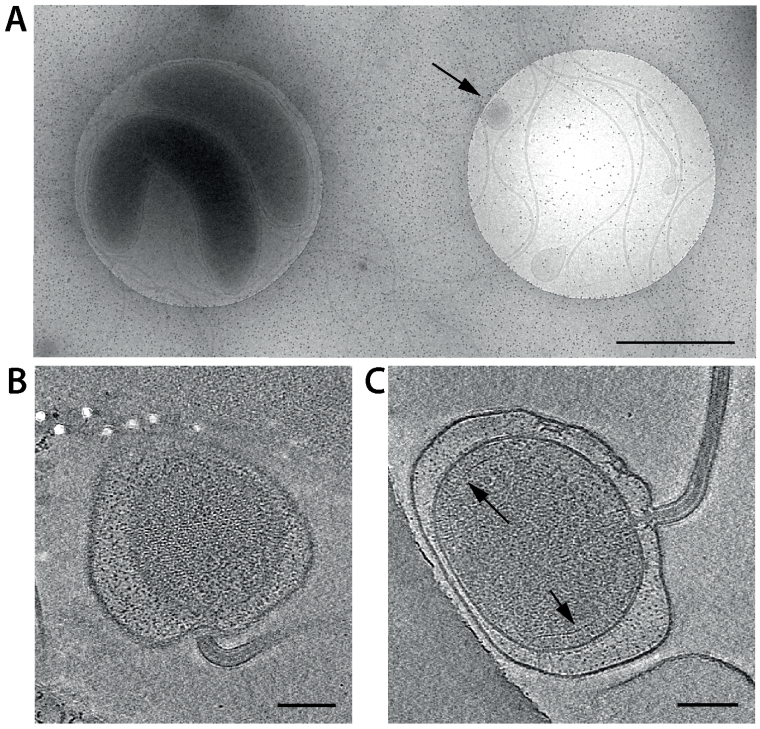

Figure 1. Representatives of *V. cholerae* minicells imaged by cryo-electron microscopy. (A) Cryo specimen of 2 regular size cells (left) and a minicell (right, indicated by an arrow) on a Quantifoil film patterned with holes. Scale bar is 1 micron. Black dots are gold nanoparticles added as fiducial markers. (B) Tomoslice of a minicell shows the hexagonal lattice. (C) Tomoslice of a minicell shows the baseplate of the chemotaxis arrays (indicated by arrows) in side view. Scale bars for panel B and C are 100 nm.

The hexagonal pattern is apparent in the cytoplasmic region of the receptors, except in regions right beneath the inner-membrane (Fig. 2B&C). The hexagonal pattern in Fig. 2B is formed through the association among receptor trimers-of-dimers. The baseplate also has a hexagonal arrangement, which corresponds to a network assembled by a variety of the chemotaxis proteins (Fig. 2D). As reported before, the receptors exhibit the typical hexagonal lattice formed by trimers-of- dimers (Fig. 2E).

Kinase can be visualized in the baseplate

Straightforward subvolume averaging of receptor hexagons does not reveal a density corresponding to the kinase. Similar to *E. coli*, the CheA in *V. cholerae* also forms homodimers. With a molecular weight of 154 kDa, the CheA dimer should be resolved and distinguishable from the major baseplate scaffolding protein CheW (18kDa monomers). Furthermore, other baseplate components, such as CheV (36kDa) and ParP (42kDa), also structurally differ significantly from CheA due to both size differences and

their sporadic presence predicted for in the wild type F6 arrays.

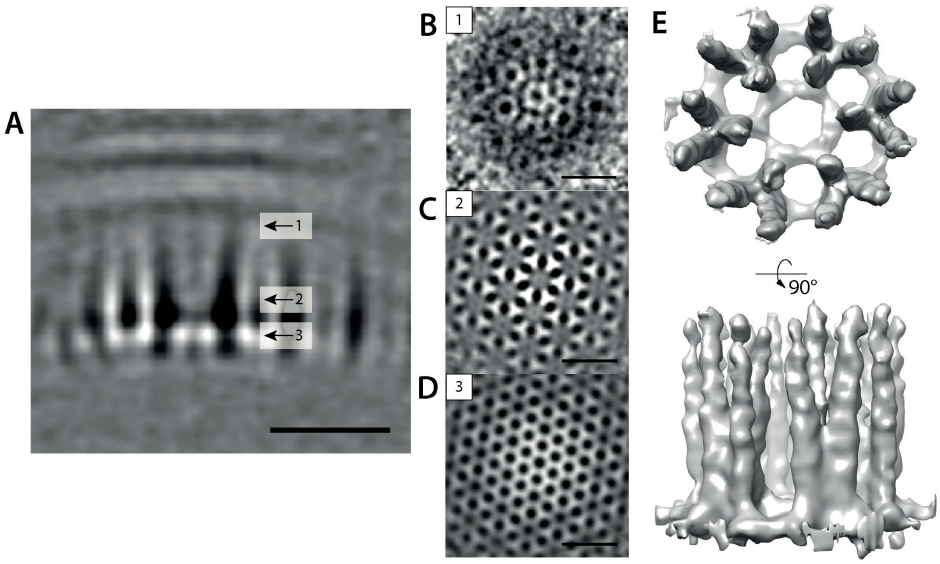

Figure 2. Subtomogram averaging result on the chemoreceptor lattice. (A) A side view of the average of receptor lattice. (B-D) Topview showing the hexagonal patter of receptor lattice at different regions indicated in panel A. (E) Isosurface rendering of the receptor hexagon average. Scale bars in all panels are 20 nm and the density is shown in white.

Based on previous results, the baseplate of F6 arrays in *V. cholerae* are expected to be different from that found in *E. coli* based on the lower abundance of CheA (102). The stoichiometry based on proteomics analysis predicts a ratio between CheA and all other baseplate proteins combined is roughly 1:6. In order to determine the location of CheA, we used principle component analysis and k-means based classification to categorize the receptor hexagons. However, the classification was not able to reveal the location of CheA. This strongly suggests that, unlike in *E. coli* where there is an alternating CheA-filled and CheA-empty ring pattern in the baseplate, the distribution of CheA in *V. cholerae* is more sporadic.

By using multi reference alignment, the receptor hexagons can be further classified into different classes with different numbers of CheAs attached beneath the receptor hexagons. For each class, the averaged volume exhibits a density that resembles CheA dimers protruding from the baseplate (Fig. 3A). The receptor arrays in *E. coli* contain a maximum of 3 CheAs per receptor hexagon. The number of CheAs in *V. cholerae* can range from 0 to 3. Noticeably, although the averages suggests there could be 3 CheAs in one of the classes, not all CheA –like densities seem to be equally robust (Fig. 3B)

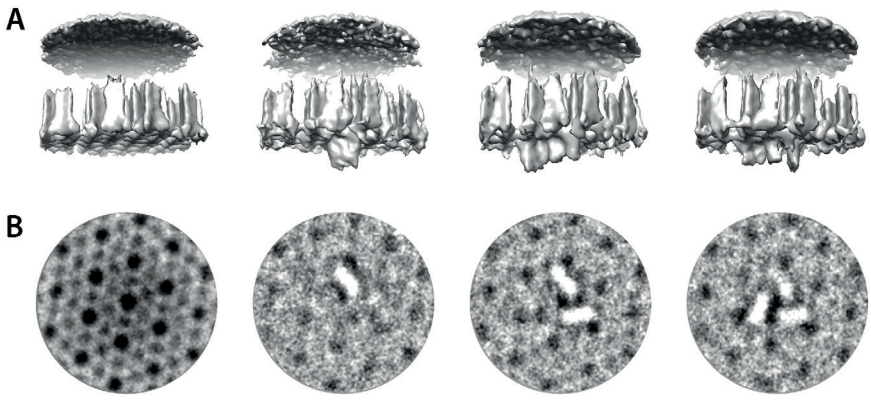

Figure 3. CheAs are visualized in classified averages base on their abundance within the baseplate. (A) Isosurfaces, from left to right, represent four classes showing 0 to 3 CheA-like densities in the bottom of the baseplate. The layer of density on top of each averaged volume corresponds to the inner membrane. (B) 2D images at the baseplate, from left to right, showing the CheA occupancy underneath the receptor hexagons.

Kinase distribute evenly yet without a pattern in baseplate

Even with CheA-like densities shown in the classification results, the individual EM maps are not informative enough to describe where the kinases are located in the context of receptor lattice. In order to visualize the location of kinase in arrays, the averages of receptors and CheAs are plotted back into the original tomograms following the coordinates and orientations derived from the iterative alignment results (Fig. 4A). Such composite volume reveals the CheA locations in the baseplates of native chemosensory arrays (Fig. 4B). Such visualization reveals that CheA is distributed evenly throughout the baseplate but lacks an ordered arrangement. This is in contrast to the highly ordered arrangement found in *E. coli*, where the baseplate is composed of alternating CheA-filled and CheA-empty rings under receptor hexagons. Instead, in the individual hexagons in *V. cholerae*, we find a variety of CheA arrangements, ranging from 0 to 3 per ring (Fig. 4C). Noticeably, in certain regions the CheA-filled and CheA-empty ring structures could still be found. However, such local CheA arrangement appeared to be extremely rare throughout a continuous chemosensory array.

Discussion

In this study, the distribution of the kinase CheA in the baseplate of intact chemotaxis cluster II arrays (F6 arrays) in *V. cholerae* was determined for the first time. We found that the CheA distribution appears evenly across the baseplate of arrays but it lacks any detectable pattern. This kinase distribution is in agreement with the low CheA

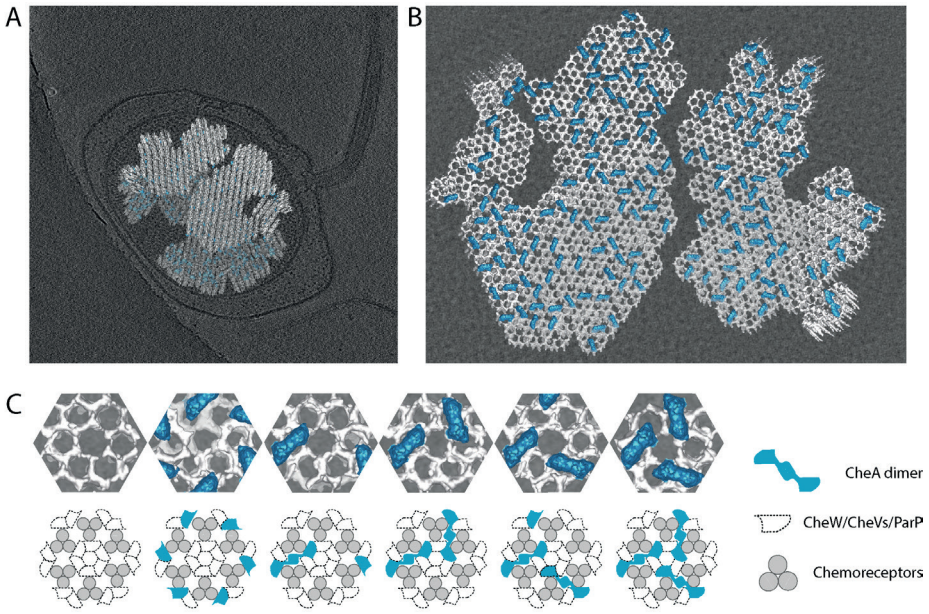

Figure 4. Atlas of a CheA distribution model in the *V. cholerae* F6 arrays. (A) A slice of a *V. cholerae* minicell tomogram where the subtomogram averaging results of chemoreceptors and CheAs are superimposed. (B) An atlas of the baseplate showing the kinase distribution on top of a tomoslice. (C) A selection of receptor hexagons with different CheA occupancies viewed from the bottom (top row), and the corresponding cartoons illustrating the compositions (bottom row).

occupancy and high array component variability determined in a previous proteomic study (102). In our previous study, the exact ratio between baseplate components and the receptors was not studied (102). However, such a ratio can be deduced. Each receptor trimers-of-dimers can provide three possible interfaces at the cytoplasmic tips for binding with any SH3-like domain in the baseplate (47). In *Vibrio*, the baseplate proteins containing SH3-like domain include the P5 domain of CheA, CheW, ParP and CheVs (100, 108, 112). Assuming a 1:1 ratio between receptor dimer and the SH3-like domain candidates, we can estimate the CheA occupancy of the receptor lattice based on the proportion of CheA among the baseplate components. The ratio between CheA-P5 to non-CheA baseplate components was previously reported to be between 1:5 and 1:7(102). This proportion implies that, approximately, one CheA homodimer is expected for two adjacent receptor hexagons. In contrast, three CheA homodimers are present per two adjacent receptor hexagons in *E. coli*.

It is difficult to calculate the exact ratio between receptors and CheAs based on the proportion of different classes after classification result. The receptor trimers-of-dimers naturally form a superlattice in which every two adjacent receptor hexagons

inevitably overlap by sharing two receptor trimers-of-dimers. As a result, a single CheA dimer connecting those two trimers-of-dimers is always shared between two receptor hexagons and thus potentially appears in more than one class in the classification process. Therefore, the percentages of individual classes do not directly reflect the absolute CheA number. In addition, the classification algorithm is not sophisticated enough to categorize all receptor hexagons with all the possible CheA arrangements with an equal certainty. In *E. coli*, receptor hexagons have either 0 or 3 CheA dimers protruding beneath the baseplate. Yet in *V. cholerae*, the receptor hexagons can contain any CheA number between 0 and 3. For the same classification algorithm, it is of lower fidelity distinguishing 3 CheAs and 2 CheAs compared to distinguishing 3 CheAs to no CheA at all. In our analysis, 52% of the receptor hexagons were classified as lacking CheA. This roughly fits with our expectation that at least 1 CheA is shared between 2 neighboring receptor hexagons based on experimentally determined stoichiometry.

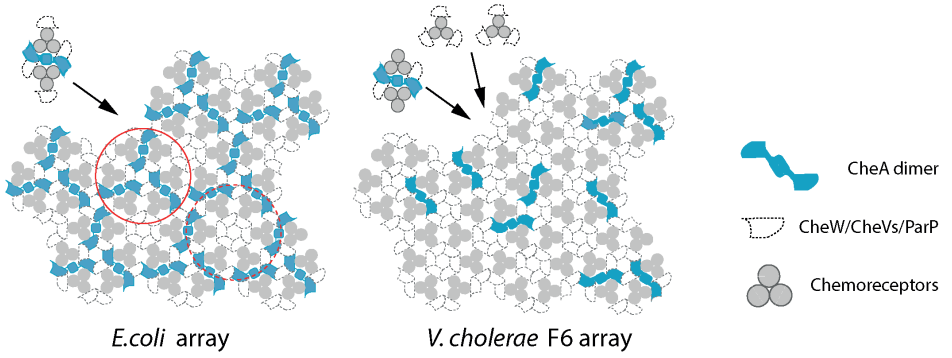

Figure 5. Models of the chemotaxis array assembly between *E. coli* (left) and *V. cholerae* (right). The CheA-filled and CheA-empty rings in *E. coli* are indicated with red circles in solid and dash lines, respectively.

Noticeably, in a few regions of one continuous receptor superlattice, we can see a continuous patch of receptors seemingly lacking CheA completely. However, it is difficult to verify whether this local array patch really completely lacks CheA. Such lack of CheAs is structurally possible, as previous results showed that extensive hexagonally packed receptor arrays could be established even in a total absence of CheA (102). Intriguingly, it is unclear how *V. cholerae* could benefit from recruiting and assembling receptors without assigning sufficient number of kinases for proper chemotaxis function. To our knowledge, CheA is the only known component that is capable of generating the output signal of the chemosensory arrays by converting the signaling information from chemoreceptors into phosphorylation of response regulators. In *E. coli*, the core unit rigidly repeats itself to form an overall ordered receptor lattice and the baseplate in such a way that each receptor trimers-of-dimer always directly communicates with a CheA (Fig. 5). In contrast, in *V. cholerae*, the seemingly random distribution and fewer

number of CheAs in the baseplate means that signals generated by some receptors would have to propagate horizontally in the baseplate for a longer distance before it can reach a nearby kinase (Fig. 5). It is unclear how robust this long distance signaling propagation could be and how it may promote the signaling cooperativity to allow kinase modulation under the collective control of a variety of receptors.

Another possible scenario for CheA-less local regions in the lattice may be due to the fact that certain receptors could prefer to bind to CheVs or ParP and those receptors are under conditional unregulated expression. The attainable resolution by cryo-ET is not sufficient for an unambiguous distinction among CheW, CheV and ParP monomers due to their similar molecular mass. Dimeric ParP (84kDa) has been proposed to integrate in the baseplate to substitute dimeric CheA (112, 146). However, ParP only accounts for 2% of baseplate components according to provious proteomics analysis. Such low abundance means that a substantially larger tomographic dataset would be needed to obtain enough ParPs in order to resolve its dimeric form *in situ*. Additionally, a much-improved resolution would also be needed for visualizing and distinguishing both CheVs and ParPs from CheWs to verify the possible clustering.

Given the universal appearance of the chemoreceptor lattice observed in a wide range of bacteria and archaea so far, the structural diversity in chemosensory arrays could easily be overlooked (51, 55). Yet, we have gradually become aware that different CheA distribution patterns in the baseplate among species is a notable feature of chemosensory arrays. In contrast, the highly conserved structural arrangement of the receptor lattice is present in all motile chemotactic bacteria and archaea examined thus far. Furthermore, *V. cholerae* is capable of assembling three independent chemosensory arrays that all share the same 12 nm spacing hexagonal packing order for the receptor lattice (104, 122). Would the other two arrays (F7 and F9 arrays) share the same kinase distribution pattern as revealed for the F6 arrays in this study? Visualization of CheA in these baseplates might help us understand how different arrays function within one species.

Material and Methods

Strains and cell culture

CheA-free *V. cholerae* was constructed as described previously (102). *V. cholerae* minicell yielding strain was engineered with minCD deletion and the matAB deletion in the genome, which gave a 1 in 20 rate of minicell generation (175) . *Vibiro* strains were received as gift from collaborators. For imaging, the *V. cholerae* minicell strain was cultured overnight in LB media at 30° with 200 rpm shaking.

Minicell cryo specimen preparation

Overnight culture of the *V. cholerae* minicells were enriched using sucrose gradient centrifugation. *V. cholerae* culture was first centrifuged at 4,000 rcf for 10 minutes. The pellets were discarded, while the supernatant was further centrifuged at 8,000 rcf for 20 minutes. The supernatant was discarded and the pellets were re-suspended in 2 ml Gelatin Saline Buffer (GSB contains 0.085% NaCl, 0.003% $KHPO_4$, 0.006%K_2HPO_4 and 10 µg/ml gelatin at pH 7.7). The cell suspension was then carefully transferred onto 40 ml sucrose gradient (5-30%) GSB. Sucrose gradient was achieved by first dissolving 12 g sucrose in 40m GSB buffer, letting it freeze completely in -20 °C and then thaw completely without stirring at 4 °C before use. After 45 minutes of spinning at 2,000 rcf, the top 4 ml of cell suspension was collected. The minicell suspension went through another 20 minutes of centrifugation at 21,000 rcf, and the pellets were re-suspended in 20 µl LB media.

Protein A coated, 10-nm gold nanoparticles solution (Utrecht University, The Netherlands) was added into the *V. cholerae* minicells suspension. After brief vortexing, 3 µl aliquots of mixture was transferred onto freshly glow-discharged R2/2, 200 mesh copper Quantifoil grid (Quantifoil Micro Tools). In climate chamber set to 20 °C and 95% humidity, the excess liquid was blotted off before the grid was plunge frozen in liquid ethane by Leica EM GP system (Leica Microsystems).

Electron microscopy

Image acquisition was performed on a Titan Krios transmission electron microscope (Thermo Fisher Scientific) operating at 300 kV equipped with a Gatan GIF Quantum K2 Summit detector with a slit width set to 20 eV (Gatan, the United States). Tilt series were collected on minicells showing flagellum clearly attached. SerialEM software package (178) was used for with a bidirectional tilt scheme that covers a tilting range between – 60 ° and 60 ° starting at 0 ° with a 2 ° increment. Defocus was set to a range between -5 to -8 microns. The magnification corresponds to 3.5 Å/pixel. Images were collected in counted mode with dose fractionation. An accumulative dosage was set to 80 e/$Å^2$ for each tilt-series.

Image processing

Alignframes from IMOD software package (179) was used for motion correction of the frames. Bead-tracking based tilt-series alignment was performed also within IMOD. CTFplotter (157) was used for defocus determination and phase-flip only contrast transfer function correction before tomogram reconstruction. Tomograms were reconstructed with weighted back-projection both with and without using SIRT-like filter of 9 iterations within IMOD, for visualization and subtomogram extraction purpose, respectively.

Dynamo software package was employed for subtomogram alignment averaging and classification analysis of the subtomograms (158, 159, 180). Visual examination first distinguished tomograms that contains *V. cholerae* minicells exhibiting chemosensory arrays. The initial template was generated from manually picked subtomograms from array lattice in the top-view. Then, subtomograms of arrays following the cell curvature and shown in side-view in the tomogram were first modeled as patch of surface and then extracted and aligned to the initial model. After the receptor hexagons were aligned coarsely, multireference alignment was performed for classification purpose with a cylinder mask that loosely enclosed the area beneath the receptor hexagon. While allowing only in-plane rotation, four types of averages were derived from the multireferences alignment representing four different possibilities of CheA distribution in the baseplate.

To visualize the overall kinase distribution beneath the receptor lattice, subboxing centering at CheA was performed for classes exhibiting CheA in the multireference alignment results. The subtomogram containing an individual CheA in the center was further aligned and eliminate duplicates based on their minimum spacing in the lattice. Finally, the isosurfaces of receptor hexagons and the CheAs were separately rendered in 3DMOD and reprojected back into the tomograms with the coordinates and orientation converted from alignment results.